Radiation Physics and Chemistry 200 (2022) 110387

Contents lists available at ScienceDirect

Radiation Physics and Chemistry

journal homepage: www.elsevier.com/locate/radphyschem

Dose rate mapping of an industrial ^{60}Co irradiator using an online photodiode-based dosimetry system

Josemary A.C. Gonçalves [a], Alessio Mangiarotti [b], Carmen C. Bueno [a,*]

[a] Instituto de Pesquisas Energéticas e Nucleares, 05508-000, Cidade Universitária, São Paulo, Brazil
[b] Instituto de Física - Universidade de São Paulo, 05508-080, Cidade Universitária, São Paulo, Brazil

ARTICLE INFO

Keywords:
Dose rate mapping
PIN photodiode Dosimeter
Radiation processing dosimetry
Gamma dosimetry

ABSTRACT

In this work, a housemade dosimetry system based on a thin photodiode is applied for online mapping of dose rates, between 2.6 and 37.7 Gy/h, delivered by a Panoramic ^{60}Co industrial facility. The operational principle of the dosimeter relies on the real-time acquisition of the induced currents from the irradiated diode operating in the short-circuit mode without externally applied voltage. The radial mapping of the radiation field is performed by rotating the diode around the central axis of the panoramic irradiator, covering 360° at intervals of 18°. The results are benchmarked with alanine dosimeters, Monte Carlo simulations, and reference dose rates retrieved from the facility calibration. The overall consistency of the whole data complies with the maximum response variation (8%, k = 2) recommended by the International Standard Protocols for routine dosimeters in radiation processing dosimetry. It reveals that the photodiode-dosimetry system is a reliable alternative to map dose rate fields and the effectiveness of Monte Carlo simulations as a predictive tool for dose rate measurements in an irradiator.

1. Introduction

In the radiation processing field, any irradiation process is designed to irradiate products uniformly, but in practice, a reasonable variation in the absorbed dose through the product is accepted. In an established process, the maximum and minimum dose recommended for a product depends on the regulatory requirements and, once determined, must be accurately delivered. So, a tight dosimetry control of the process is paramount, and it has been routinely accomplished by several well-established dosimeters, such as ferrous sulfate and ceric-cerous solutions, alanine, polymethylmethacrylate (PMMA) materials, and radiochromic films (ICRU Report 80, 2008, ISO/ASTM 51702, 2013; ISO/ASTM 52628, 2020). However, the irradiation of inhomogeneous or irregularly shaped products gives rise to complex dose variations posing challenges for the quality assurance of the dosimetry. Although time-consuming, the usual approach to tackle this issue is mapping the dose in the product using chemical dosimeters that measure the integral dose after the irradiation ends (Sephton et al., 2007; Mortuza et al., 2018). Real-time dosimeters based on ionization chambers, diodes, and transistors with prompt and easy readout might be most suitable for dose mapping (Oliveira et al., 2000; Fuochi et al., 2004; Sephton et al., 2007; Bailey et al., 2009; Andjelković and Ristić, 2013, 2015; Majer et al., 2019). Ionization chambers are intrinsically radiation-resistant, but the measurements must be corrected for temperature, pressure, and humidity. In addition, as ionization chambers are less sensitive than semiconductor devices, they require larger volumes for the same detection efficiency, worsening the spatial resolution.

Diodes and transistors are prone to radiation damage giving rise to a sensitivity drop with accumulated dose. This damaging effect shortens the dose lifespan of both devices, but diodes, with a simpler structure and operating principle, are favorably compared to transistors (Santos et al., 2002; Spezzigu, 2010; Paschoal et al., 2011; Andjelković and Ristić, 2013). However, regardless of the silicon device type, their lifespan, smaller than a few kGy, constraints their widespread use in radiation processing applications where doses of tens of kGy are easily achieved. The endorsement of this statement stems from the pioneering feasibility studies of using diode-based dosimeters for monitoring and mapping gamma radiation fields (Muller, 1970a, b; Osvay et al., 1975; Möhlmann, 1981; Dixon and Ekstrand, 1982). In general, they report a lack of response stability due to variations induced in the current sensitivity by radiation damage and inhomogeneities of electrical characteristics of the devices due to manufacturing technology failures.

* Corresponding author. Av. Lineu Prestes 2242, Cidade Universitária, 05508-000, São Paulo, SP, Brazil.
E-mail address: ccbueno@ipen.br (C.C. Bueno).

https://doi.org/10.1016/j.radphyschem.2022.110387
Received 8 March 2022; Received in revised form 27 June 2022; Accepted 1 July 2022
Available online 14 July 2022

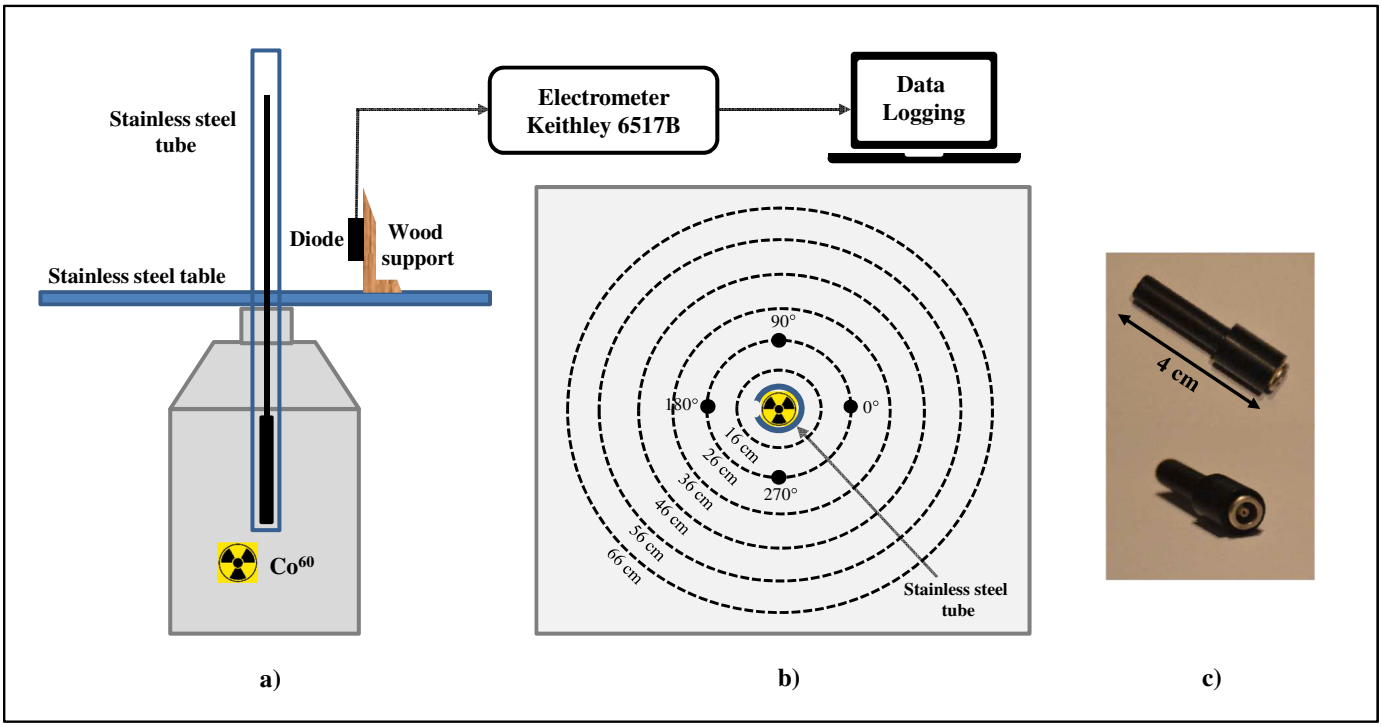

Fig. 1. a) Schematic diagram of the experimental setup; b) Top view of the circles engraved on the tabletop, angular pattern, and the cut view of the cylindrical source guide with an opening opposite to the reference irradiation position at 0°; c) Photograph of the dosimetric probe.

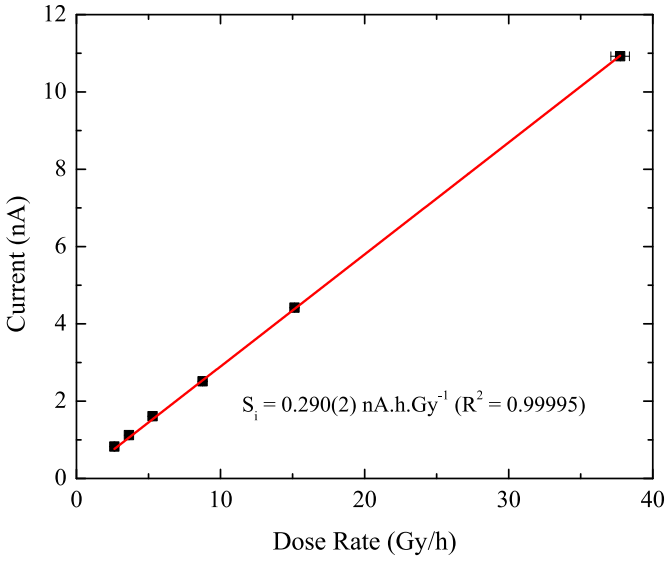

Fig. 2. Dose rate response of the diode placed at 0° and 10 cm above the tabletop. The current sensitivity of 0.29 nA h/Gy is assessed through the slope of the plot.

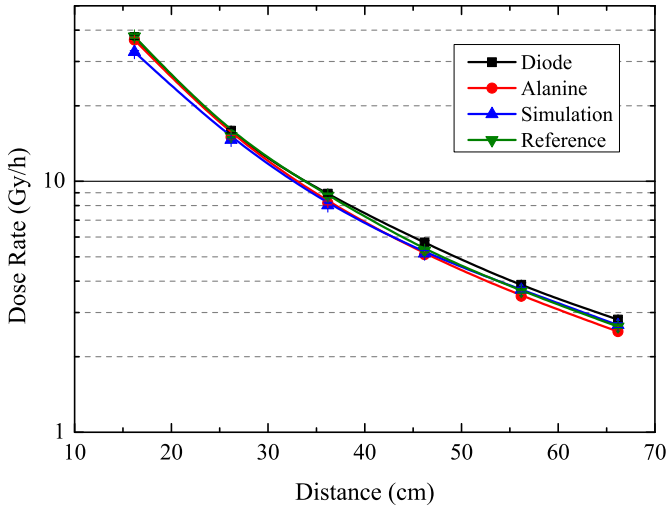

Fig. 3. Data from diode and alanine dosimeters positioned at 0° as a function of the dosimeter-source distance. For comparison, simulations and reference dose rates retrieved from the facility calibration are plotted together. The plot is on a logarithmic scale to aid data visualization.

For this reason, diodes are neither recommended for high-dose radiation processing dosimetry (ISO/ASTM 51702, 2013; ISO/ASTM 52628, 2020) nor are routinely used in large-scale industrial facilities to the best of our knowledge.

However, great efforts have been made by the high-energy physics community toward enhancing the radiation hardness of silicon diodes (Lindström, 2001; Casati et al., 2005; Härkönen et al., 2005; Bruzzi et al., 2007; Moll, 2018) which have brought back the interest in using diode-based dosimeters for high-level dosimetry. In this line of investigation, promising results from some radiation-hard diodes operating in the current mode have been obtained and published elsewhere (Bueno et al., 2022). The main contribution of this dosimetry system is the capability for online dose measurements of cents of kGy since there are plenty of well-established passive dosimeters for high-dose applications (ICRU Report 80, 2008). Nevertheless, despite the outstanding lifespan (>300 kGy) and wide operational dose range (5–275 kGy) of these diodes, they are not appropriate for mapping static gamma fields of about a few cents of Gy (Bueno et al., 2022). However, the increasing trend of new radiation processes, for sanitary purposes and biological materials, with doses of only a few tens of Gy, has evidenced a lack of suitable routine dosimeters, except alanine and radiochromic films, covering such a low-dose range. For these applications, our recent work (Gonçalves et al., 2020, 2022) has shown that a thin photodiode-based

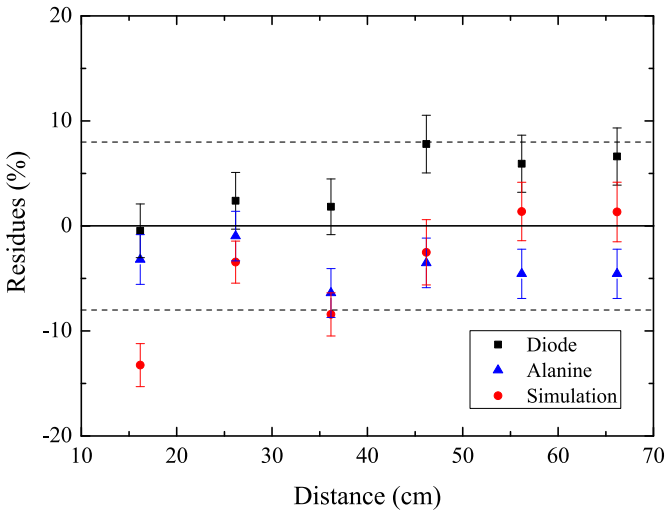

Fig. 4. Residues of the experimental and simulated dose rate data related to the reference dose rate values from the facility calibration. The error bar of each residue is given by the propagation of the uncertainties related to the corresponding experimental/calculated data and reference values. The zero on the vertical scale represents the reference dose rate values. Dashed lines show the maximum allowed response variation (8%, k = 2) of routine dosimeters for radiation processing dosimetry.

dosimeter operating in active or passive modes has the response stability and dosimetric characteristics required for the quality control of radiation processing dosimetry. It also meets the basic requirements of large availability, cost-effectiveness, and ease of operation, enabling its deployment as a routine dosimeter in industrial radiation processing facilities. In continuity with this line of investigation and for the sake of completeness, it is proposed to investigate the real-time performance of the photodiode for dose rate mapping in a small-scale industrial ^{60}Co panoramic irradiator. This facility has been dedicated to establishing new radiation processes and low-dose biomedical research activities. For these applications, the dose rate assessment in different points of the irradiation field is essential for fulfilling dose requirements by optimizing the exposure time of products with different shapes and densities. The results obtained are benchmarked with alanine measurements and Monte Carlo simulations.

2. Experimental setup

A homemade dosimetry system based on a p-i-n photodiode (SFH206K, OSRAM) is used in this work. The device bears a 7.02 mm^2 active area, small capacitance (72 pF at 0V), and dark currents less than 1 pA. It is assembled in a light-tight dosimetric probe with the frontal p-layer directly connected to the Keithley 6517B electrometer and grounded n-backplane. Details of the dosimetric probe construction and the diode electrical characterization can be found elsewhere (Gonçalves et al., 2020, 2022). The dosimetric principle of this system relies on the real-time acquisition of the radiation-induced current signals from the diode operating in the short-circuit mode without externally applied voltage. Offline integration of the current signals gives the corresponding absorbed dose. A schematic diagram of the detection system and a photograph of the dosimetric probe are shown in Fig. 1.

The irradiations are performed with the ^{60}Co gamma rays from a Panoramic irradiator (FIS 60–04, Yoshizawa Kiko Ltd), consisting of a 20 cm long radioactive pencil double shielded 4 mm thick stainless steel blades. The source is enclosed in a lead vessel stored under a square stainless steel table 150 cm wide and 120 cm in height above the floor level. Six circles (radii 16–66 cm and 1 mm thick), concentric with the axes of the radioactive pencil, are engraved on the stainless steel tabletop to define the irradiation position precisely. This geometry allows products and dosimeters to be irradiated at different distances from the ^{60}Co source, covering dose rates from 2.6 to 37.7 Gy/h. Such dose rates were previously calibrated through standard reference alanine dosimeters (1.7%, k = 2) with traceability to the secondary standard laboratory at the International Atomic Energy Agency (IAEA).

The dose-rate response, i.e., the current signal reading as a function of the reference dose rate, is assessed at 0° and 10 cm above the irradiation tabletop by changing the diode-source distance from 16 to 66 cm. At each distance, three consecutive current measurements, lasting 300 s each, are carried out by switching on and off the irradiator. The

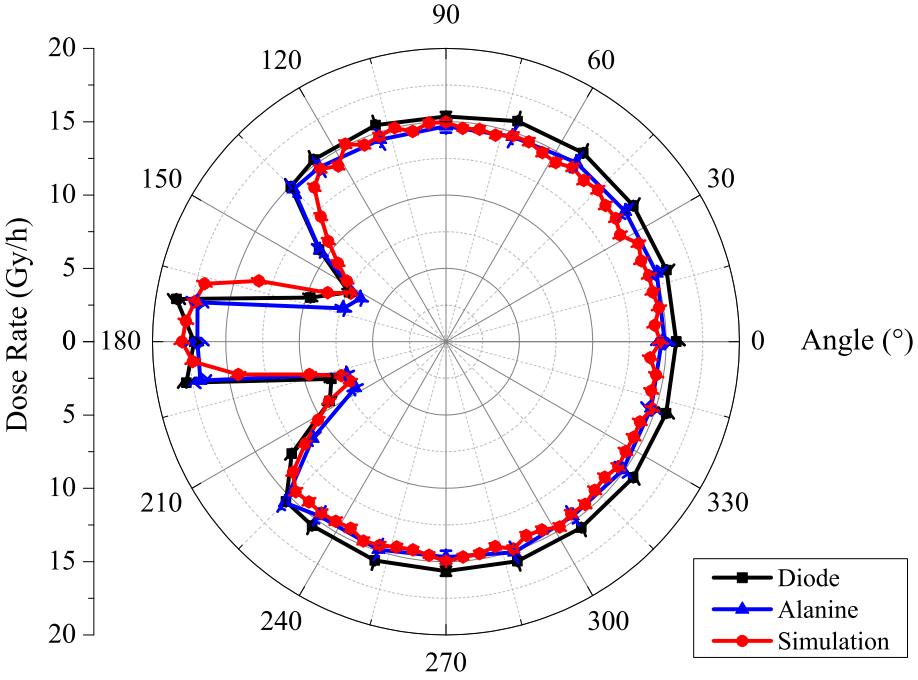

Fig. 5. Dose rate mapping of the Panoramic ^{60}Co gamma irradiator predicted and measured with diode and alanine dosimeters 26 cm away from the radioactive source.

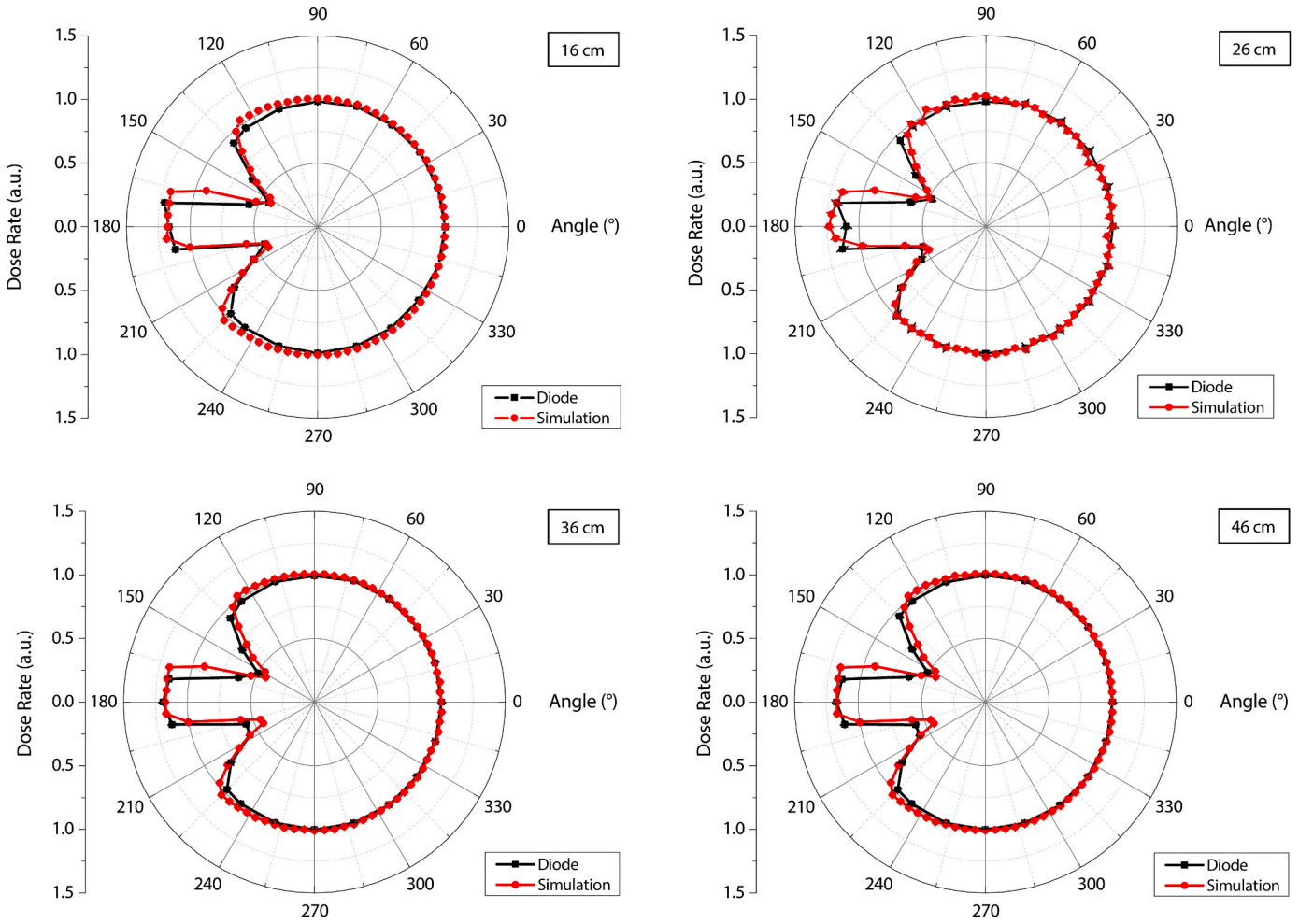

Fig. 6. Predicted dose rate mapping of the Panoramic ^{60}Co gamma irradiator and measurements carried out with the diode positioned at a) 16 cm, b) 26 cm, c) 36 cm, and d) 46 cm away from the radioactive source. Each dose rate value is normalized to that obtained at 0° to highlight the dose rate profile matching.

Keithley 6517B electrometer performs the current readings under 16.67 ms integration time, selected to provide the best compromise between the acquisition speed of the current signals and noise. A time interval of 0.5 s between two readings is set to account for the buffer storage capacity and the exposure time. For analyses, the data are sent to a personal computer via the GPIB interface controlled by software developed in Labview. During the measurements, it is possible to convert the current reading to dose rate using the calibrated current sensitivity parameter previously attained under the same experimental conditions (Gonçalves et al., 2022). It allows real-time monitoring of irradiation. A type K thermocouple monitors the room temperature (22 ± 1) °C during the exposure time.

The dose-rate mapping of the radiation field is performed at different diode-source distances. At each distance, the diode is rotated around the central axis of the panoramic irradiator, covering 360° at intervals of 18°. Three current readings are sequentially assessed during 300 s each at the same angle. The expanded uncertainties (k = 2) of the current measurements derive from the diode reading (statistical errors less than 0.5%), the electrometer accuracy (0.3%), the diode positioning (0.5%), and temperature variation (0.4%).

Alanine dosimeters, composed of 93% alanine and 7% binder, 4.0 mm diameter and 2.2 mm thick (Aerial, France), are also employed to map the panoramic radiation field to benchmark the data assessed with the diode-based dosimeter. Three alanine pellets, are placed side-by-side, spaced 1.5 mm apart in an acrylic phantom kept at 10 cm above the irradiation tabletop and 26 cm away from the source. At this distance, the reference dose rate (15.14 Gy/h) enables the absorbed dose to be achieved within the operational dose range of alanine (0.01–100 kGy) at a reasonable exposure time (1.5 h). Irradiations are performed to almost 25 Gy in each angular position ranging from 0° to 360° in steps of 18°. The center-to-center distance between the pellets is 7.5 mm, leading to maximum variations of ±2.7° at each incidence angle. The spectrum acquisition is performed with an MS400 ESR spectrometer (Magnettech, Berlin) equipped with the AerEDE dosimetry software (Aerial, France). The measurement parameters are properly adjusted to 8 mW microwave power, magnetic field centered at 3370 G with 30 G field sweep, ten scans with a sweep time of 12 s, a gain of 100, and 180° phase. The spectrometer readings are converted to dose through the alanine calibration curve (ISO/ASTM 51607, 2013), obtained earlier under the same parameters, covering the range of 5–100 Gy. The dose to the exposure time ratio results in the corresponding dose rate. The expanded uncertainties of the dose rate are given by the data fitting of the calibration curve (2.2%) and the irradiation time (0.5%).

3. Simulations

The steps necessary to perform simulations with a general purpose Monte Carlo package are generally three: a) describe the geometry of the setup, b) initialize the primary particles, and c) score the energy deposition according to the intended result. The Geant 3 (Application Software Group, 1994) Monte Carlo has been chosen for the present work because steps b and c were already available from our previous (unpublished) studies. The Geant Low Energy Compton Scattering (GLECS) extension by Kippen (2004) has been substituted to the standard Geant 3

description of Rayleigh and Compton scattering to include the effect of electron binding in atoms. In fact, the Klein-Nishina energy transfer cross-section can underestimate the correct result for 10 keV photons by a factor of approximately 3 (Ribberfors and Berggren, 1982; Brusa et al., 1996).

The ^{60}Co source is accurately described, including the allowed (99.88%) and the second forbidden (0.12%) beta transitions. Although the major interest here relies on photons, the beta particles are considered since they can produce bremsstrahlung photons mostly in the ^{60}Co pencil and double shields. The spectra are calculated with the EFFY code by Garcia-Toraño and Garcia-Toraño and Grau Malonda (1981, 1985) according to the Fermi theory with shape corrections for the Coulomb attraction. These spectra are read at initialization time by a user routine in Geant 3, and the decay branch and energy sampled accordingly. The gamma rays emitted in the de-excitation of Nickel are then generated considering the most intense transitions: one 1.173 MeV (99.85%) followed by one 1.333 MeV gamma for the allowed decay, and one 1.333 MeV gamma (99.98%) for the second forbidden decay. The angular distribution of the beta particles and gamma rays is isotropic, disregarding angular correlations.

The geometry of the setup is included, considering the following parts. The source is formed by the ^{60}Co pencil and two layers of steel shielding. The irradiator comprises the table, a reinforcement of stainless steel on the floor, and the source storage vessel made of lead. The cylindric stainless steel guide of the source with its rails (having one opening on the backside, see Fig. 1) is also included. Finally, the room with the floor and ceiling of concrete and the reinforcement steel piles are also implemented. The necessary dimensions have been taken from the blueprints supplemented by some on-site measurements. The source can not be accessed, and all the parameters are taken from the manufacturer certificate. While the source materials and the cylindric guide are crossed in transmission geometry by the gamma rays, the other volumes are necessary to account for backscattering correctly. Finally, the diode silicon volume, aluminum metallization, and lucite probe are also included. The detector has the shape of a ring surrounding the source at the correct distance so that one simulation covers all the azimuthal angles at once.

The Monte Carlo evaluates the dose deposited in the silicon material of the diode directly. However, most photons just pass through it without interacting, requiring a large number of histories to be simulated. The results obtained employ $4{\cdot}10^9$ ^{60}Co decays, only at the closest position of 26 cm, requiring approximately 64 days of CPU time on the last generation multi-core 64-bit unit running at 2.3 GHz (EPYC 7352 manufactured by AMD®). Considering all distances, three times as many events have been run in total. Then, it is possible to calculate the dose per ^{60}Co decay for the position of the diode closest to the source with an uncertainty of 1% for a 5-degree angular bin. The results obtained multiplied by the activity of the radioactive source give the dose rate.

4. Results and discussion

Fig. 2 shows the current data as a function of the reference dose rate spanning from 2.6 to 37.7 Gy/h. Each point value is the average of three consecutive measurements. The results reveal that the dose rate response linearly depends on the current signals with a (0.290 ± 0.002) nA.h/Gy current sensitivity. This parameter, assessed through the slope of the plot, agrees well with the sensitivity previously obtained with the same diode in a similar dosimetric probe (Gonçalves et al., 2022).

Using this sensitivity parameter, the current readings from the diode settled at 0°, and different distances (d) to the radioactive source, are properly converted to dose rates.

These results are benchmarked with the data assessed with alanine dosimeters in the same angular position (0°) and distances used for the diode. The experimental and simulated values of the dose rates, with the reference ones retrieved from the dosimetric calibration of the irradiator, are depicted in Fig. 3 for comparative purposes. Across all data, the diode readings are slightly higher than those from the alanine dosimeters. This consistent discrepancy might be ascribed to the differences between the dosimeter sizes, thus covering distinct regions in the radiation field with non-negligible dose rate gradients. Thus the dose absorbed by the tiny diode is expected to be higher than the average dose absorbed by the three pellets assembly. Such differences are a significant source of uncertainties when comparing dosimetry systems (Sephton et al., 2007; Bailey et al., 2009; Majer et al., 2019). It also explains the underestimated values of the dose rate of alanine dosimeters compared to the reference dose rate data. These discrepancies in the dose rate assessment with the three pellets assembly are very likely due to the experimental approach, which is inappropriate despite being the only feasible in industrial facilities. Alanine is a gold-standard reference dosimeter, thereby ideal for validating the performance of other routine dosimeters. It is corroborated by the recent characterization of the diode used in this work, whose dose readings match those assessed with alanine by 2% (Gonçalves et al., 2022).

Fig. 3 also shows the good agreement among the simulations, the reference dose rates, and the experimental data from both dosimeters. The overall consistency of the simulations and the experimental data sets is evidenced in Fig. 4, where the corresponding residues to the reference dose rates are presented.

Except for the simulated dose rate value in the region closest to the radioactive source, where a high gradient dose rate occurs, the whole data is within the maximum allowed response variation (8%, $k = 2$) of routine dosimeters for radiation processing dosimetry (ICRU Report 80, 2008; ISO/ASTM 51702, 2013; ISO/ASTM 52628, 2020).

An inspection of Fig. 4 reveals that the simulation agrees well with the expected and measured dose rates for the farthest positions of the diode. For the closest positions, the distance of 36 cm and especially that of 16 cm show systematic underestimations. The latter is rather outside the expected uncertainty. The accuracy of these simulations, besides the physical interaction mechanisms and the cross-section library (which are expected to cause an error insensitive to the dosimeter position), mainly depends on the reliable input data concerning the structural details of the source and the industrial facility, which is always complex and can give rise to position-dependent inaccuracies. Mortuza et al. (2018) have also simulated a semi-industrial ^{60}Co irradiation facility with MCNP transport code and found that the irradiation field region close to the source is the most difficult to reproduce correctly. The further away from the source, the less the details of its construction matter and the lower the gradient of the irradiation field is. We, therefore, attribute the problems observed close to the source to inaccuracies in the description of the source or the facility, pending future investigations, if the issue becomes relevant for routine operation.

The assessment of the dose rate distribution is performed only for dosimeter-source distances from 26 cm to 46 cm to exclude the closest position, with the largest discrepancy, and the two outmost ones, where statistical fluctuations in the simulations are larger. For the shortest distance of this range, the data from both dosimeters and the predicted dose rates are depicted in Fig. 5. The dose rate profiles are very similar, revealing the effect of the opening made in the cylindrical tube to install the rails that guide the source between shielding and irradiation position. Except for this region, which is never used for irradiating products due to the high dose rate gradient, all data agree with the experimental uncertainties. Despite this, the good matching of the simulated dose rate profiles to those attained with the diode is revealed in Fig. 6, where each dose rate value is normalized to that obtained at 0°. The low dose rates at larger dosimeter-source distances preclude time-consuming measurements with alanine. It corroborates the utmost advantage of the diode dosimeter, which, besides ease of handling and low cost (2 dollars each), bears good spatial resolution (2.7 mm) and fast current response (16.67 ms). With these features, diodes are good alternatives for dose rate mapping, mainly for a detailed survey of the nonuniform radiation field in panoramic irradiators.

Nevertheless, the SFH206K diode lifespan, 15 kGy for ^{60}Co gamma

rays (Gonçalves et al., 2020), restricts its use only in small-scale gamma irradiators.

5. Conclusion

The use of a homemade diode-based dosimetry system for dose rate mapping of a small-scale ^{60}Co Panoramic irradiator has been investigated in this work. The results are benchmarked with alanine dosimeters, Monte Carlo simulations, and reference dose rate data. The overall consistency of the whole data complies with the maximum response variation (8%, k = 2) recommended by the International Standard Protocols for routine dosimeters in radiation processing dosimetry. The good features of the diode dosimeter, mainly regarding the prompt measurements (16.67 ms), good spatial resolution (2.7 mm), and ease of handling, endorse its reliable use for dose rate mapping of nonuniform gamma radiation fields.

Credit authors statement

J. A. C. Gonçalves: Methodology, Formal analysis, Investigation, Resources, Data Curation, Funding acquisition, Review & Editing.

A. Mangiarotti: Methodology, Formal analysis, Review & Editing.

C. C. Bueno: Conceptualization, Methodology, Formal analysis, Writing - Original Draft, Writing - Review & Editing, Supervision.

Declaration of competing interest

The authors declare that they have no known competing financial interests or personal relationships that could have appeared to influence the work reported in this paper.

Data availability

Data will be made available on request.

Acknowledgments

The authors highly acknowledge the collaboration of Eng. Elisabeth S. R. Somessari from the Gamma Irradiators staff (IPEN-CNEN/SP) for her indispensable help during the irradiations. This work is partially supported by IPEN-CNEN/SP (DPDE Edital 04/2017) and CNPq (contracts nº 306331/2016–0 and 311915/2020–5). Computational resources were made available by FAPESP under contract nº 2016/13116–5.

References

Andjelković, M.S., Ristić, G.S., 2013. Feasibility study of a current mode gamma radiation dosimeter based on a commercial PIN photodiode and a custom made autoranging electrometer. Nucl. Technol. Radiat. Protect. 28 (1), 73–83, 10.2298NTRP/1301073A.

Andjelković, M.S., Ristić, G.S., 2015. Current mode response of phototransistors to gamma radiation. Radiat. Meas. 75, 29–38. https://doi.org/10.1016/j.radmeas.2015.03.005.

Bailey, M., Sephton, J.P., Sharpe, P.H.G., 2009. Monte Carlo modeling and real-time dosemeter measurements of dose rate distribution at a ^{60}Co industrial irradiation plant. Radiat. Phys. Chem. 78 (3), 453–456. https://doi.org/10.1016/j.radphyschem.2009.03.024.

Brusa, D., Stutz, G., Riveros, J.A., Fernández-Varea, J.M., Salvat, F., 1996. Fast sampling algorithm for the simulation of photon Compton scattering. Nucl. Instrum. Methods A 379, 167.

Bruzzi, M., Bucciolini, M., Casati, M., Menichelli, D., Talamonti, C., Piemonte, C., Svensson, B.G., 2007. Epitaxial silicon devices for dosimetry applications. Appl. Phys. Lett. 90, 172109 https://doi.org/10.1063/1.2723075.

Bueno, C.C., Camargo, F., Gonçalves, J.A.C., Pascoalino, K., Mangiarotti, A., Tuominen, E., Härkönen, J., 2022. Performance characterization of dosimeters based on radiation-hard silicon diodes in gamma radiation processing. Frontiers in Sensors 3, 770482. https://doi.org/10.3389/fsens.2022.770482.

Casati, M., Bruzzi, M., Bucciolini, M., Menichelli, D., Scaringella, M., Piemonte, C., Fretwurst, E., 2005. Characterization of standard and oxygenated float zone Si diodes under radiotherapy beams. Nucl. Instrum. Methods 552, 158–162. https://doi.org/10.1016/j.nima.2005.06.025.

Dixon, R.L., Ekstrand, K.E., 1982. Silicon diode dosimetry. Int. J. Appl. Radiat. Isot. 33, 1171–1176.

Fuochi, P.G., Lavalle, M., Corda, U., Recupero, S., Bosetto, A., Baschieri, V., Kovács, A., 2004. In-plant calibration and use of power transistors for process controlo f gamma and eléctron beam facilities. Radiat. Phys. Chem. 71, 383–386. https://doi.org/10.1016/j.radphyschem.2004.03.034.

Garcia-Toraño, E., Grau Malonda, A., 1981. EFFT, a program to calculate the counting efficiency of beta particles in liquid scintillators. Comput. Phys. Commun. 23, 385.

Garcia-Toraño, E., Grau Malonda, A., 1985. EFFY, a new program to compute the counting efficiency of beta particles in liquid scintillators. Comput. Phys. Commun. 36, 307.

Gonçalves, J.A.C., Mangiarotti, A., Bueno, C.C., 2020. Current response stability of a commercial PIN photodiode for low dose radiation processing applications. Radiat. Phys. Chem. 167, 108276–108279. https://doi.org/10.1016/j.radphyschem.2019.04.026.

Gonçalves, J.A.C., Mangiarotti, A., Bueno, C.C., 2022. Characterization of a thin photodiode as a routine dosimeter for low-dose radiation processing applications. Radiat. Phys. Chem. 198, 110200–110206. https://doi.org/10.1016/j.radphyschem.2022.110200.

Härkönen, J., Tuovinen, E., Luuka, P., Tuominen, E., Li, Z., Ivanov, A., Verbitskaya, E., Eremin, V., Pirojenko, A., Riihimaki, I., Virtanen, A., 2005. Particle detectors made of high-resistivity Czochralski silicon. Nucl. Instrum. Methods 541, 202. https://doi.org/10.1016/j.nima.2005.01.057.

ISO/ASTM 51607, 2013. Practice for Use of the Alanine-EPR Dosimetry System. https://doi.org/10.1520/ISOASTM51607-13.

ISO/ASTM 51702, 2013. Standard Practice for Dosimetry in a Gamma Facility for Radiation Processing, 3.

ISO/ASTM 52628, 2020. Standard Practice for Dosimetry in Radiation Processing, 2.

Kippen, R.M., 2004. The GEANT low energy Compton scattering (GLECS) package for use in simulating advanced Compton telescopes. N. Astron. Rev. 48, 221.

Lindström, G., 2001. Radiation hard silicon detectors developments by the RD48 (ROSE) Collaboration. Nucl.Instr.Methods A 466, 308. https://doi.org/10.1016/S0168-9002(01)00560-5.

Majer, M., Roguljić, M., Knežević, Z., Starodumov, A., Ferenček, D., Brigljević, V., Mihaljević, B., 2019. Dose mapping of the panoramic ^{60}Co gamma irradiation facility - GEANT4 simulation and measurements. Appl. Radiat. Isot. 154, 108824 https://doi.org/10.1016/j.apradiso.2019.108824.

Möhlmann, J.H.F., 1981. The use of solar cells for continuous recording of absorbed dose in the product during radiation sterilization. In: Biomedical Dosimetry, Proceedings of Symposium. IAEA Publication STI/PUB/567, Vienna, p. 563, 1981.

Moll, M., 2018. Displacement damage in silicon detectors for high energy physics. IEEE Trans. Nucl. Sci. 65 (8), 1561–1582. https://doi.org/10.1109/TNS.2018.2819506.

Mortuza, Md F., Lepore, L., Khedkar, K., Thangam, S., Nahar, A., Jamil, H.M., Bandi, L., Alam, Md K., 2018. Commissioning dosimetry and in situ dose mapping of a semi-industrial Cobalt-60 gamma-irradiation facility using Fricke and Ceric-cerous dosimetry system and comparison with Monte Carlo simulation data. Radiat. Phys. Chem. 144, 256–264. https://doi.org/10.1016/j.radphyschem.2017.08.022.

Muller, A.C., 1970a. The "n" on "p" solar-cell dose-rate meter. In: Holm, N.W., Berry, R.J. (Eds.), Manual on Radiation Dosimetry, p. 423. New York.

Muller, A.C., 1970b. The "p" on "n" solar-cell integrating dosimeter. In: Holm, N.W., Berry, R.J. (Eds.), Manual on Radiation Dosimetry, p. 429. New York.

Oliveira, C., Salgado, J., Carvalho, A.F., 2000. Dose rate determinations in the Portuguese Gamma Irradiation Facility: Monte Carlo simulations and measurements. Radiat. Phys. Chem. 58 (3), 279–285. https://doi.org/10.1016/S0969-806X(99)00462-4.

Osvay, M., Stenger, V., Földiak, G., 1975. Silicon detectors for measurement of high exposure rate gamma rays. In: Biomedical Dosimetry, Proceedings of Symposium. IAEA Publication STI/PUB/401, Vienna, p. 623, 1974.

Paschoal, C.M.M., Sobrinho, M.L., Souza, D.N., Antonio Filho, J., da Silva Junior, E.F., Santos, L.A.P., 2011. Characterization of three photodetector types for computer tomography dosimetry. In: Proceedings of the World Academy of Science, Engineering and Technology Conference.

Report 80, I.C.R.U., 2008. International Commission on Radiation Units and Measurements, Dosimetry Systems for Use in Radiation Processing, ICRU Report 80 (International Commission on Radiation Units and Measurements. https://doi.org/10.1093/jicru/ndn031, 2008.

Ribberfors, R., Berggren, K.F., 1982. Incoherent-X-ray-scattering functions and cross sections (dσ/dΩ)incoh by means of a pocket calculator. Phys. Rev. 26, 3325.

Santos, L.A.P., da Silva Jr., E.F., Vilela, E., 2002. Filtered X ray beam dosimetry from 10^{-3} to 10^{2} Gy dose range by using phototransistors. Radiat. Protect. Dosim. 101 (1–4), 145–148. https://doi.org/10.1093/oxfordjournals.rpd.a005956.

Sephton, J.P., Sharpe, P.H.G., Chu, R.D.H., O'Hara, K.P.J., Abdel-Rehim, F., Abdel Fattah, A., 2007. Dose mapping of a ^{60}Co industrial irradiation plant using an electronic data recording system, static measurements, and mathematical modeling. Radiat. Phys. Chem. 76 (11), 1820–1825. https://doi.org/10.1016/j.radphyschem.2007.02.110.

Software Group, Application, 1994. GEANT 3: A Detector Description and Simulation Tool. CERN Program Library Long Writeup (CERN, Geneva), p. W5013.

Spezzigu, P., 2010. Reliability Investigations of Bipolar Silicon Phototransistor Arrays for Space Applications. Ph.D. thesis. University of Cagliary.